Journal of Advanced Joining Processes 12 (2025) 100354

Contents lists available at ScienceDirect

Journal of Advanced Joining Processes

journal homepage: www.sciencedirect.com/journal/journal-of-advanced-joining-processes

Exploring the hybridization of wire-arc additive manufacturing and resistance spot welding

Maria R.F. Barros [a], Pedro M.S. Rosado [a], Rui F.V. Sampaio [a], João P.M. Pragana [a], Ivo M.F. Bragança [b], Carlos M.A. Silva [a], Paulo A.F. Martins [a,*]

[a] IDMEC, Instituto Superior Tecnico, Universidade de Lisboa, Lisboa, Portugal
[b] CIMOSM, Instituto Superior de Engenharia de Lisboa, Instituto Politécnico de Lisboa, Portugal

ARTICLE INFO

Keywords:
Hybrid manufacturing
Wire-arc additive manufacturing
Resistance spot welding
Experimentation
Finite element method

ABSTRACT

This paper explores a new hybrid manufacturing approach that combines wire-arc additive manufacturing (WAAM) with resistance spot welding (RSW). The approach integrates additively deposited materials with commercial sheets, which can serve as either supporting or functional elements. Experimental testing and finite element modelling allowed defining the weld lobe and optimizing key parameters such as electric current and welding time. Optimization was based on nugget shape, microstructure, and mechanical performance from destructive shear and peel tests. Two distinct joining modes were identified: symmetric and asymmetric weld nuggets, with the former exhibiting higher strength but requiring a higher heat input. A proof-of-concept prototype was developed to demonstrate the potential of this innovative hybrid manufacturing approach, combining WAAM, machining, forming, and RSW to fabricate complex, multi-thickness components with improved structural integrity.

Introduction

The concept of hybrid manufacturing began to gain prominence in both academic and industrial discussions in the early 2010s. A significant milestone occurred when Lauwers et al. (2014) presented a keynote paper at the International Academy for Production Engineering (CIRP) General Assembly entitled ‘Hybrid Processes in Manufacturing’. In this pioneering work, they offered a widely cited definition of hybrid processes, describing them as ‘those based on the simultaneous and controlled interaction of process mechanisms and/or energy sources/tools having a significant effect on the process performance’.

This definition encapsulates the essence of manufacturing innovation: the ability to combine two or more distinct processes in a controlled and coordinated way, leading to an outcome that exceeds the sum of its parts. This principle is sometimes summarized by the expression ‘$1 + 1 = 3'$, which illustrates the idea of synergy, where combining different energy sources, tools, or mechanisms results in a performance boost that goes beyond incremental improvements. Rather than simply adding capabilities together, hybrid processes transform manufacturing possibilities, paving the way for innovative product designs.

The requirement for simultaneous interaction of processes, as described in the CIRP keynote paper by Lauwers et al. (2014), sparked significant debate among CIRP members during 2012 and 2013 while the paper was being discussed and prepared. This debate prompted some CIRP members, including Zhu et al. (2013), to propose a broader definition of hybrid manufacturing, arguing that the sequential interaction between two or more processes should also be considered. This broader definition asserts that combining manufacturing processes can provide benefits and capabilities that are unattainable through any single process, thereby classifying any combination of two or more processes as hybrid, regardless of whether they operate simultaneously or sequentially.

Over the last few years, several authors have explored the integration of metal additive manufacturing (MAM) with conventional manufacturing processes to unlock new design possibilities, enhance production efficiency, and create complex geometries that cannot be achieved through the hybridization of conventional processes alone

* Corresponding author.
E-mail addresses: ritabarros@tecnico.ulisboa.pt (M.R.F. Barros), pedro.s.rosado@tecnico.ulisboa.pt (P.M.S. Rosado), rui.f.sampaio@tecnico.ulisboa.pt (R.F.V. Sampaio), joao.pragana@tecnico.ulisboa.pt (J.P.M. Pragana), ivo.braganca@isel.pt (I.M.F. Bragança), carlos.alves.silva@tecnico.ulisboa.pt (C.M.A. Silva), pmartins@tecnico.ulisboa.pt (P.A.F. Martins).

https://doi.org/10.1016/j.jajp.2025.100354

Available online 10 October 2025

(Merklein et al., 2016). Pragana et al. (2021) provide a comprehensive overview of the ongoing developments in the field, highlighting applications resulting from the hybridization of MAM with machining, forming, and joining by forming processes.

Recent studies published in the literature have examined the combination of MAM with conventional welding processes, including laser welding (Matilainen et al., 2016; Mokhtari et al., 2021), gas metal arc welding (Selmi et al., 2023; Braun et al., 2023), gas tungsten arc welding (Huysmans et al., 2021), and resistance spot welding (RSW) (Kim et al., 2023). However, these studies focus primarily on additively manufactured parts created through powder bed fusion (PBF) processes, which utilize laser or electron beam power sources. As a result, the findings are often limited in size, require expensive equipment and feedstock materials, and typically involve extensive post-processing operations to remove support structures. Additionally, since PBF processes must operate under controlled atmosphere conditions, integrating welding or other manufacturing operations during the layer-by-layer building process is largely restricted, meaning such operations can only occur in the post-processing stage.

The potential of hybridizing conventional welding processes with direct energy deposition (DED) techniques, particularly those within wire-arc additive manufacturing (WAAM), remains underexplored. WAAM is widely regarded as more suitable for constructing large components due to its higher deposition rates and improved material efficiency (Ucsnik and Kirov, 2011; Rosado et al., 2024). Unlike PBF processes, WAAM does not require a closed, controlled atmosphere chamber. This significantly reduces one of the main barriers to process integration, allowing for the direct execution of complementary manufacturing operations, such as machining (Li et al., 2023), rolling (Gornyakov et al., 2022), and peening (Sitharaj et al., 2024) during the deposition process.

It is worth noting that, to date, there have been no attempts to hybridize WAAM with RSW. In this context, this paper explores the potential benefits of combining WAAM and RSW to meet the industrial demands for the production of large-scale, complex metal parts. The primary objective is to facilitate the integration of various combinations of conventionally manufactured wrought thin metal sheets and additively deposited metals during layer-by-layer construction using resistance spot welding (see Fig. 1).

This is demonstrated with the presentation of a proof-of-concept prototype that showcases the effectiveness of this innovative hybrid manufacturing approach, successfully combining WAAM, machining, forming, and RSW to fabricate a complex metal part with variable thickness. Experimental and finite element modelling of RSW under unit cell level supports the presentation and enables the optimization of key welding parameters, such as electric current and welding time.

Material and methods

Wrought and deposited materials

The combination of WAAM with RSW involved the creation of lap joints using 1 mm commercial wrought AISI 316 sheets and 3 mm AISI 316 L stainless steel samples obtained from material deposition and milling.

The material was deposited using an ESAB Luc Aristo 400 gas metal arc welding power source in combination with a 3-axis CNC router table. A 1 mm diameter AISI 316 L stainless steel wire supplied by ESAB was fed through the welding torch and melted in a spray transfer mode onto hot rolled AISI 316 L baseplates with 20 mm thickness. The spray transfer mode was selected to achieve high deposition rates and to prevent potential cold lapping defects between the deposited material and the initially cold baseplate.

The deposition process involved single-bead, multiple-layer deposition sequences along straight linear paths with varying starting points for each layer to build vertical walls with small lateral reinforcements. These reinforcements were intended to enhance overall stiffness and minimize the impact of thermally induced distortion on the baseplates (referred to as the ‘substrate’). The resulting material layers had an average width and height of 6 mm and 1.25 mm, respectively. The main parameters used in material deposition were optimized from the author’s previous work (Pragana et al., 2023) and are summarized in Fig. 2a.

The resulting walls shown in Fig. 2b and 2c measured approximately 200 mm in height, 200 mm in length, and 5 mm in thickness. After material deposition, the lateral reinforcements were removed, and the walls were milled to achieve a uniform thickness of 3 mm. Rectangular samples, roughly measuring 20 mm by 25 mm, were intentionally extracted from the walls to avoid any preferential directions and to minimize the grain size orientation in the deposited material caused by WAAM. The samples were then ground with P80 grit sandpaper for use in subsequent RSW operations involving unit cells of the lap joints in the experiments.

Resistance spot welding

The welding tests were carried out in a TECNA® 810X resistance welding machine equipped with a TE500 weld control unit operating at 50 Hz. The electric current during welding varied between 6 kA to 12 kA, while the welding times ranged from 1 to 30 cycles of 20 milliseconds each. The electrode force was constant throughout the experiments with a value of 4.0 kN.

The electrodes used in the welding experiments were nearly pure electrolytic copper (99.9 %) and shaped like truncated cones with a flat circular contact surface measuring 8 mm in diameter, in accordance with the specifications of the ISO 5182 standards (International Organization for Standardization 2016a)

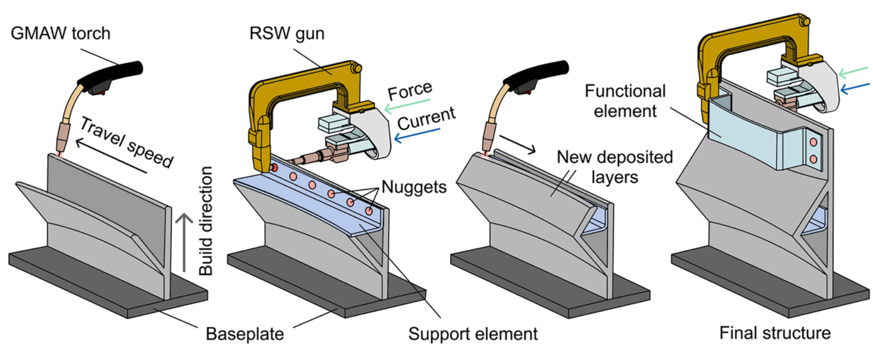

Fig. 1. Schematic representation of a potential application of the new proposed hybrid manufacturing approach that integrates wire-arc additive manufacturing with resistance spot welding (RSW).

Current (A)	100
Voltage (V)	16.5
Wire feed speed (m/min)	6
Travel speed (m/min)	0.6
Shielding gas	Ar (99.99%)
Gas flow rate (l/min)	10
Layer height (mm)	1.25
Stickout distance (mm)	10

(a)

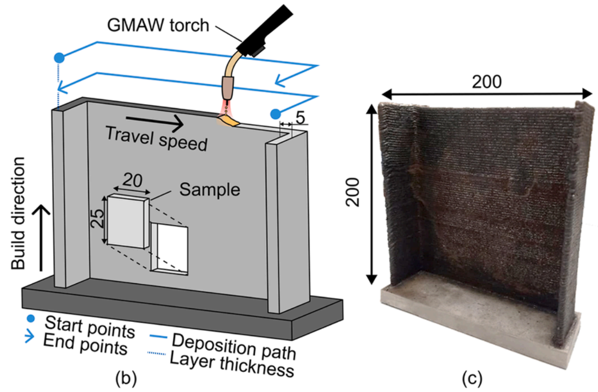

Fig. 2. Deposition of AISI316L stainless steel by WAAM. (a) Summary of the main process parameters. (b) Schematic representation of the deposition strategy used for building the walls and (c) photograph of one as-built wall. Dimensions in (b) and (c) are in millimetres.

Fig. 3a shows a schematic representation of the experimental setup with the two overlapping sheets positioning between the electrodes. The setup was designed to capture the welding force, electric current, and voltage effectively. It includes a TECNA® 1460 force analyser strategically positioned underneath the lower electrode to measure the welding force, a Rogowski coil and a TECNA®1430 weld tester located around the lower electrode base to measure the current, and a Pico® 'Differential Probe' equipped with spring-loaded hooks connected to each electrode base, for voltage measurement (Fig. 3b).

All three devices were connected to an oscilloscope, allowing for real-time monitoring, data storage, and export. The oscilloscope (illustrated in Fig. 3a) was set up to trigger when there was an increase in electrode force. This configuration effectively captured the entire welding process while ignoring the time it took for the electrodes to approach the sheets, as no force is applied until contact is made (Calado et al., 2022).

Finite element modelling of resistance spot welding

The RSW of the lap joints made from 1 mm commercial wrought and 3 mm deposited AISI 316 L stainless steel sheets was simulated using the finite element commercial software SORPAS®. The simulation focused on the influence of the two main process parameters, electric current and welding time, which were evaluated using the following threefold strategy.

The first step involved configuring the RSW process within the SORPAS® simulation environment by identifying the rigid objects (electrodes) and the plastically deforming objects (sheets and interface layers), as shown in Fig. 4a. Additionally, the material interfaces representing the contact properties between the overlapping sheets and between the sheets and electrodes were modelled with a thickness of 0.05 mm to replicate the roughness of the contacting surfaces

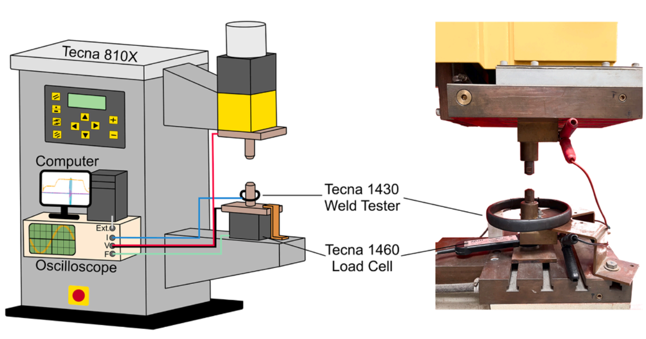

Fig. 3. (a) Schematic representation and (b) close-up photograph of the experimental setup utilized in RSW.

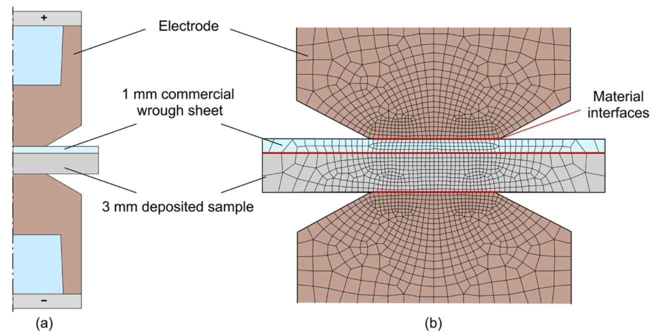

Fig. 4. (a) Electrodes, sheets, and interface layers, and (b) the corresponding finite element model for resistance spot welding.

(SWANTEC, 2019).

The thermo-mechanical behaviour of these interfaces was aligned with the average properties of the stainless steel and electrolytic copper surfaces, along with an electric resistivity ρ_c^e that depends on the normal pressure p_n applied at the contact areas between each two adjacent surfaces,

$$\rho_c^e = \frac{C}{\sqrt{p_n}} \tag{1}$$

In the above equation, C is a constant that depends on the surfaces and processing conditions, as explained in a previous work of the authors (Sampaio et al., 2023)

The second step involved specifying the simulation type as staggered thermo-electrical mechanical (Zhang, 2003), and the third and final step was to build the finite element model. This was done by discretizing the material of the two sheets positioned within and adjacent to the welding region with a non-structured mesh of 1000 axisymmetric quadrilateral elements (Fig. 4b). The electrodes were also discretised with axisymmetric quadrilateral elements, using the ISO 5182 electrode type selected from SORPAS database.

The material properties used in the simulations were obtained from the SORPAS database. Specifically, the properties of both WAAM-deposited and wrought AISI 316 L stainless steel were made identical.

The average computation time for the simulations was approximately 10 min on a computer equipped with an Intel i7–5930 K CPU processor. During simulation, SORPAS® provides the temperature distribution, the weld nugget diameter at the interface, the intensity level (low, medium, or high) of any splash, and the geometry of the solidified weld nugget. The predicted diameter of the weld nugget was measured at the interface, which indirectly indicates the area where the sheets are bonded.

The simulations were performed with varying values for electric current and welding time to predict the weld lobe, along with the corresponding parameters, which were then validated through experimental tests.

Microscopic observations and destructive tests

The welding nuggets produced by resistance spot welding between wire-arc deposited and commercial stainless steel were analysed by cutting the lap joints, composed of 1 mm commercial wrought and 3 mm deposited AISI 316 L sheets, through their centre. The resulting cross-sections were polished and chemically etched using Kalling's No 2 solution to observe and measure the geometry and dimensions of the melted volumes using a Mitutoyo TM-1005B low-magnification microscope.

The observations aimed to correlate the welding parameters with the standard design requirements for the corresponding welding nuggets. This involved examining the welding nugget cross-section to evaluate whether its interface diameter met or exceeded the minimum requirement of 3 mm, as recommended by the AWS C1.1M/C1.1:2019 AMD1 of the American Welding Society (2019) and the Society of Automotive Engineers (SAE), considering the thickness of the AM sheet used in the RSW process. Additionally, careful attention was given to the nugget's aspect ratio, emphasizing the importance of maintaining a minimum height-to-diameter ratio of 0.3.

Another crucial factor is to ensure that the welding nuggets remain singular rather than being separated into multiple nuggets to achieve a robust and continuous weld without compromising the structural integrity of the joints. Additionally, it is important to avoid excessive melting near the electrodes or any material expulsion.

The microstructure analysis was conducted using a Motic BA310MET-H high-magnification microscope. To assess the maximum forces that resistance spot welded (RSW) joints can safely withstand, destructive tensile shear and peel tests were performed. The dimensions for each test were selected in accordance with the standards outlined in ISO 14273:2016 (International Organization for Standardization 2016c) for tensile shear tests and ISO 14270:2016 (International Organization for Standardization 2016b) for tensile peel tests. These tests were carried out at ambient temperature using an INSTRON 4507 universal testing machine.

Results and discussion

Numerical and experimental weld lobe

Fig. 5 shows the numerically predicted weld lobe for resistance spot-welded lap joints made from 1 mm commercial wrought and 3 mm deposited AISI 316 L stainless steel sheets. It outlines the different combinations of welding current and time that result in either acceptable or unacceptable welds. The simulations were performed using the finite element software SORPAS, which allowed for the identification of three distinct regions within the weld lobe:

- The central green region represents the combinations of current and time that produce acceptable welds,
- The blue region indicates low heat input parameters, which can lead to failures due to insufficient melting at the contact interface or the formation of small nuggets,
- The red region indicates high energy input parameters, leading to the ejection of molten material from the welding region (also known as 'expulsion') or to nuggets with a diameter-to-height ratio exceeding 0.3;

The images labelled from 'A' to 'F' in Fig. 5 were retrieved from the different regions within the weld lobe to show examples of the predicted temperature distributions and the final cross-sectional shapes of the weld nuggets, with the latter represented in grey. For instance, weld nugget 'A' does not meet the minimum required interface diameter of 3 mm. Weld nugget 'C' has an excessive volume of melted material near the lower electrode which is a clear indicator of electrode sticking. Weld nugget 'D' fails to meet the minimum height-to-diameter ratio of 0.3, while weld nugget 'F' is inadequate because it has separated into multiple nuggets, as shown by the multiple regions coloured in grey.

As previously mentioned, acceptable welds must have a minimum interface diameter of 3 mm and consist of a single, cohesive nugget without signs of discontinuity along the melted volume. Additionally,

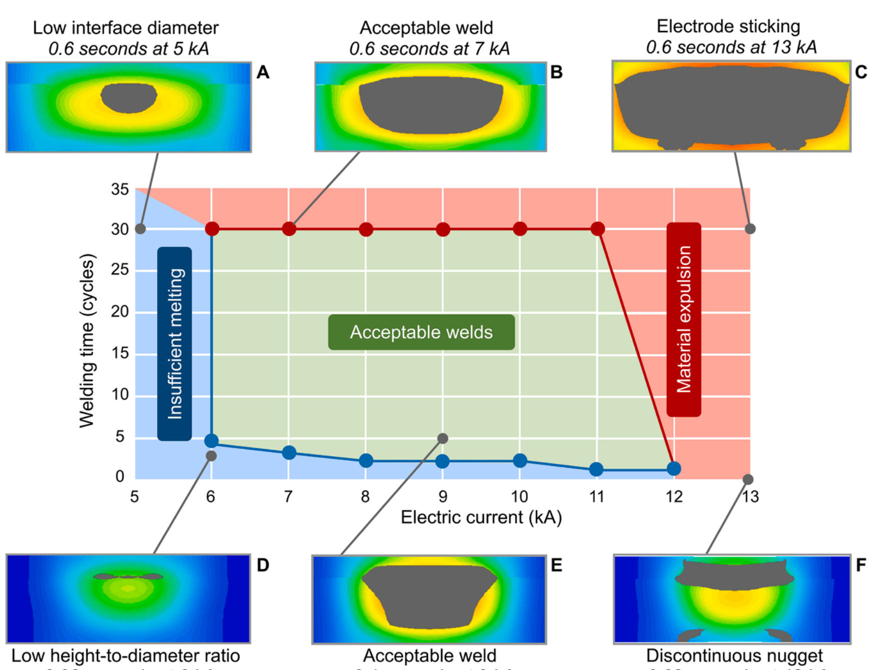

Fig. 5. Finite element predicted weld lobe resulting from a welding time ranging from 0 to 35 cycles and an electric current ranging from 5 to 13 kA. Note: The grey regions in the simulation results represent the molten volume (weld nugget).

there should be a minimum molten area near the electrode, and the ideal weld should display a symmetrical nugget shape, as shown by weld nuggets 'B' and 'E' in Fig. 5.

Fig. 6 discloses the experimental weld lobe obtained from observations and measurements. The experiments began by defining the limits of the weld lobe, starting with the lower limit, since this range of parameters is most likely to produce unsuccessful welds due to insufficient heat input. Four sets of parameters failed to make a successful joint, primarily due to a lack of fusion or an inadequate nugget diameter.

Once the lower limit was established, the tests progressed to evaluating the upper limit parameters. All tests conducted at this stage were successful and helped define the complete range of the weld lobe. The parameters previously identified as insufficient for producing satisfactory joints were confirmed to result in non-welded workpieces. Additionally, the lack of overloaded joints at the upper limits of welding time and electric current further validated the numerically predicted weld lobe graph (refer to Fig. 5).

Five unsuccessful welds at the lower limit of welding time (refer to the triangle markers in Fig. 6) indicate insufficient heat input leading to inadequate interface diameter, in contrast to the successful welding predictions obtained by finite elements analysis with SORPAS. These discrepancies are attributed to the material properties of the deposited material, which likely differ from those retrieved from the simulation software's database.

A total of seventeen experiments were carried out within the experimental weld lobe. By analysing the shape and characteristics of the weld nugget cross-sections, two distinct welding modes, referred to as "joining modes 1 and 2," were identified. Each region on the weld lobe was categorized based on specific welding parameters, allowing for the identification of transition zones between these areas. This approach enabled the prediction of the weld's joining mode, as illustrated in Fig. 6.

Joining mode 1 produces smaller, more asymmetric weld nuggets with a concave geometry, characterized by a gradual decrease in diameter from the interface to the opposite edge of the deposited sheet. This behaviour stems from short welding times, leading to a lower heat input during the welding process than to that experienced in joining mode 2. This effect ends up limiting the creation of a uniform weld nugget (Pouranvari, 2011) due to heat dissipation to the remaining deposited material and to the copper electrodes. The upper micrographs show grain coarsening near the fusion boundaries of both the commercial sheet and the deposited material, indicating localized melting followed by rapid directional solidification. This phenomenon is evidenced by the presence of narrow columnar grains extending toward the centre of the weld (Lippold and Kotecki, 2005).

In contrast, joining mode 2 produces more uniform and near symmetrical weld nuggets, characterized by having a more consistent diameter throughout the entire thickness of the welded joint. This enhanced uniformity is mostly due to higher welding times that allow increasing the heat input and consequently melt a larger volume of the deposited material compared to joining mode 1, creating to nuggets with a higher diameter.

The micrographs reveal coarse dendritic grains at the centre of the weld nugget, which can be attributed to slower cooling rates and longer solidification times. Furthermore, the heat-affected zone appears coarser, reflecting the effects of sustained high temperatures during the welding process (Mazar Atabaki et al., 2016).

Both joining modes show that the cross-sectional geometries predicted by finite element simulations using SORPAS are in good agreement with those obtained from metallographic observations.

Destructive testing of the lap joints

Lap joints created through the hybridization of WAAM and RSW were subjected to destructive testing to evaluate how the geometry of the weld nugget influences their failure mechanisms under high loads (Fig. 7). Based on the weld lobe presented in the previous section, three sets of welding parameters were selected for the destructive tests (see Fig. 6): one replicating joining mode I (9 kA, 10 cycles), and two corresponding to joining mode II (9 kA, 20 cycles and 11 kA, 20 cycles), with increasing values for electric current and welding time to assess their effect on the mechanical performance of the joints. To ensure repeatability, four repetitions were performed for each test condition.

The results indicate that the maximum force values remained

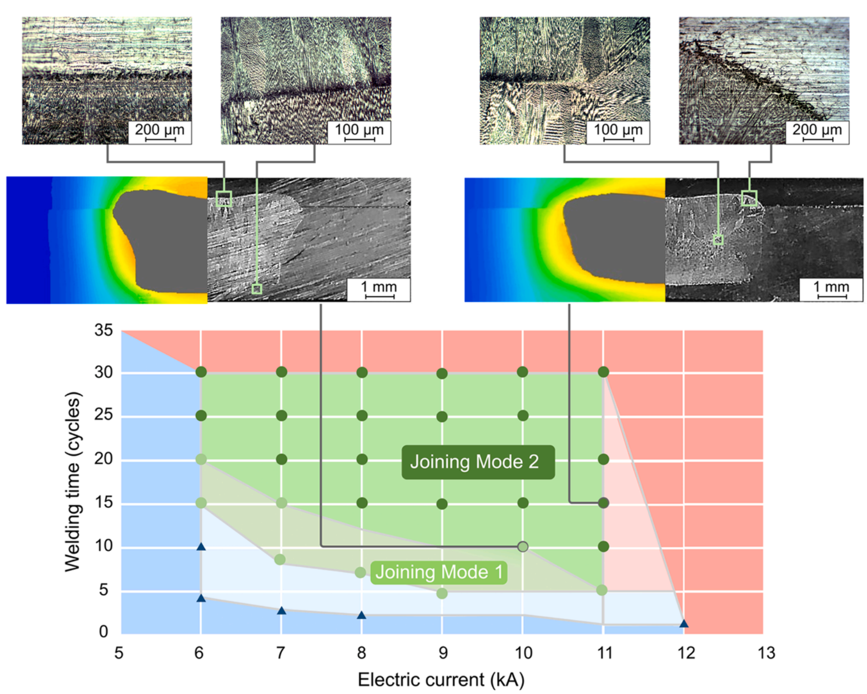

Fig. 6. Experimental weld lobe. Pictures show cross-section details of two representative weld nuggets obtained from finite elements and metallographic observations.

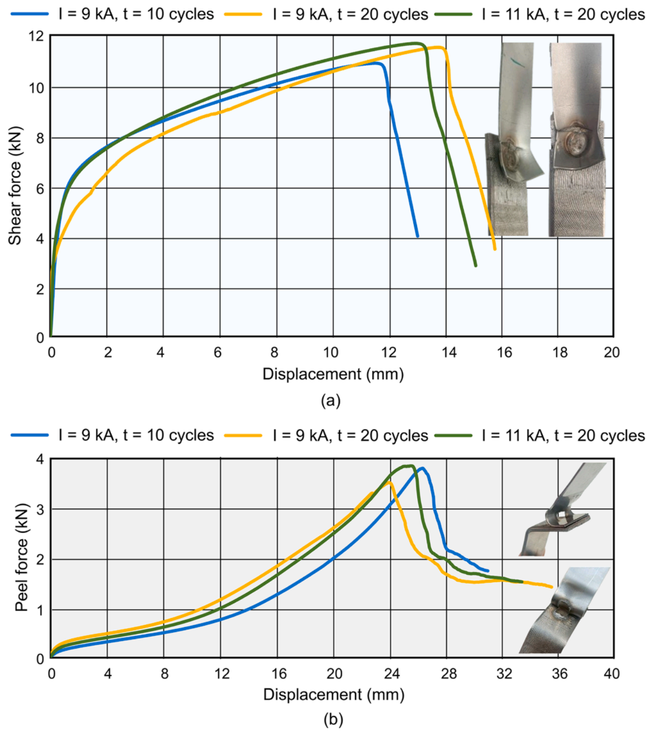

Fig. 7. Force vs. displacement evolution during (a) shear and (b) peel tests with photographs of the corresponding failure modes.

consistent across all unit cells, regardless of their weld nugget geometries and distinct microstructures. This can be attributed to a balance between geometric and microstructural factors. On one hand, the geometry of the nugget, whether it is axisymmetric or has a symmetric spot-shaped, affects how the load is transferred across the joint, helping to maintain a relatively uniform stress distribution. On the other hand, although there are variations in the microstructure within the weld zone, these differences are not substantial enough to change the dominant failure mechanisms observed during testing. Consequently, the combined effect allows the microstructural differences to be effectively "averaged out" by the weld geometry and testing conditions, resulting in comparable overall performances under shear and peel forces.

The maximum shear force ranged from 11.0 kN to 11.8 kN (see Fig. 7a), while the maximum peel force varied between 3.5 kN and 3.9 kN (refer to Fig. 7b). These findings confirm that the strength of the new joining process is comparable to that observed in other studies that utilized resistance welding to join AISI 316 L stainless steel sheets of similar thickness (Jagadeesha, 2017). In this study, a minimum of three tests were conducted per joint, and the deviations in maximum force for joints produced under the same welding parameters were approximately 0.3 kN, demonstrating a high reproducibility and consistency of the results.

The photographs in Fig. 7 provide insight into the failure modes of the joints. Their analysis shows that failure occurred due to a pull-out fracture in the heat-affected zone (HAZ) surrounding the weld areas during shear and peel tests. This indicates that the strength of the weld nugget itself is not the primary cause of failure.

The lap joints created with an electric current of 11 kA and a welding time of 20 cycles, which corresponds to Joining Mode 2 (see Fig. 6), exhibited the highest strength in both shear and peel tests. As illustrated in Fig. 7, increasing the welding time does not improve resistance to destructive forces as effectively as increasing the electric current does. This is attributed to the larger nugget diameter that results from the increased heat input.

Proof-of-concept prototype

After establishing the welding conditions needed to combine the 3 mm additive manufacturing (AM) material with the 1 mm commercial wrought stainless-steel sheets, the authors decided to explore the potential for producing complex metal components with varying thicknesses by incorporating other conventional manufacturing technologies.

Fig. 8 presents a proof-of-concept prototype that demonstrates a practical hybrid manufacturing approach that effectively combines metal deposition through wire-arc additive manufacturing (WAAM), metal cutting via milling, metal forming, and resistance spot welding (RSW) to create a complex metal part with varying thickness.

The benefits of the novel hybrid manufacturing approach, as shown in Fig. 8, extend well beyond the proof-of-concept prototype because it was specifically designed to address the challenges associated with producing complex parts that are difficult to create using traditional wrought metals and conventional manufacturing processes, or solely through existing additive manufacturing techniques, which rely only on additive and subtractive capabilities. For a part like the one in Fig. 8, conventional manufacturing typically involves the use of wrought sheets and plates, along with a combination of multiple forming operations and resistance spot welding to shape and assemble the various components into a final part. Additionally, machining the desired truncated eight-lobe conical shape would be particularly challenging due to its very thin walls (below 0.6 mm) and sharp concave corners.

Fig. 8a depicts the conceptual design and dimensions, while Fig. 8b presents photographs showcasing the integration of machining, forming, and RSW of both the wrought and deposited stainless steel materials.

The forming operation utilized single-point incremental forming to shape a commercially wrought sheet into an eight-lobe geometry. The machining operations focused on the additively manufactured (AM) material to enhance the metallic bonds between the two materials. These machining operations included the separation of the as-built walls from the substrate and the final tuning of the two main channels located in the bottom part of the component.

In resistance spot welding (RSW), the parameters used consisted of an electric current of 11 kA and a welding time of 20 cycles. These settings derived from the numerical and experimental results previously obtained for Joining Mode 2 (see Fig. 6), which were found to produce the strongest joints, as demonstrated by the highest strength observed in both shear and peel destructive testing.

Conclusions

This paper explored the combination of wire-arc additive manufacturing (WAAM) and resistance spot welding (RSW) to develop innovative hybrid manufacturing routes, including machining and forming, to produce complex parts with varying thicknesses.

The following key conclusions can be drawn:

- The investigation demonstrated that AISI 316 L stainless steel, deposited using WAAM, can be successfully joined to commercially wrought AISI 316 sheets through RSW. This finding establishes the viability of this hybrid manufacturing approach for creating lap joints in multi-thickness metal structures,
- Two distinct types of welding nuggets were identified: symmetric and asymmetric. Symmetric nuggets, typically formed under higher heat inputs, resulted in coarser grain structures and more uniform nugget geometries. In contrast, asymmetric nuggets were associated with finer grain structures originating from lower heat inputs. Despite these differences, they were not impactful enough on the mechanical performance of the joints under shear and peel loads, which remained similar for both types of nuggets and consistent with results from the literature attained from conventional RSW joints on austenitic stainless-steel alloys,

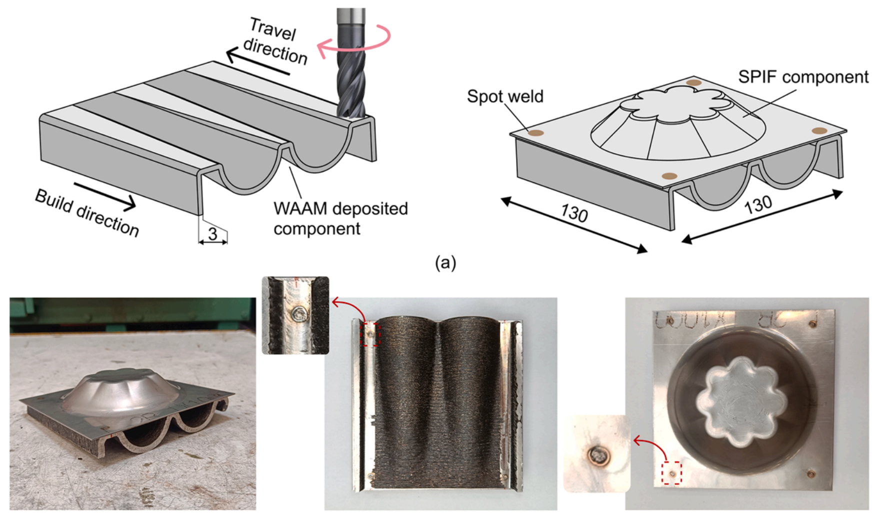

Fig. 8. The proof-of-concept prototype showing: (a) the conceptual drawings and dimensions (in millimetres) of the AM deposited along with the final assembled part, and (b) details of the upper and lower parts produced with the various processes involved in the hybrid manufacturing approach.

- Finite element simulations conducted using SORPAS® accurately predicted the weld lobe graph and the nugget morphology, confirming its effectiveness as a reliable tool for process optimization. Minor discrepancies between the numerical predictions and experimental results were mainly found for low heat input values and were attributed to differences in the material properties of the additively manufactured components compared to those listed in the software's database,
- Destructive shear and peel tests indicated that the hybrid joints exhibited mechanical strength comparable to conventional RSW made from monolithic wrought stainless-steel sheets. Failure typically occurred in the heat-affected zone of the thinner wrought sheet rather than within the weld nugget, which signifies adequate joint integrity,
- A proof-of-concept prototype successfully integrated WAAM, machining, forming, and RSW, demonstrated the industrial potential of this new hybrid manufacturing approach for fabricating robust, geometrically complex components with variable thicknesses.

In summary, the hybridization of WAAM and RSW presents new opportunities for the cost-effective production of structurally sound metal components, particularly in applications that require tailored geometries and localized reinforcements.

CRediT authorship contribution statement

Maria R.F. Barros: Writing – review & editing, Visualization, Validation, Software, Investigation, Data curation. **Pedro M.S. Rosado:** Writing – review & editing, Validation, Methodology, Investigation, Data curation. **Rui F.V. Sampaio:** Writing – review & editing, Validation, Methodology, Investigation, Data curation. **João P.M. Pragana:** Writing – review & editing, Visualization, Validation, Resources, Methodology, Investigation, Data curation, Conceptualization. **Ivo M.F. Bragança:** Writing – review & editing, Validation, Methodology, Investigation, Data curation, Conceptualization. **Carlos M.A. Silva:** Writing – review & editing, Validation, Supervision, Resources, Project administration, Methodology, Investigation, Funding acquisition, Conceptualization. **Paulo A.F. Martins:** Writing – original draft, Validation, Resources, Project administration, Funding acquisition, Conceptualization.

Declaration of competing interest

The authors declare that they have no known competing financial interests or personal relationships that could have appeared to influence the work reported in this paper.

Acknowledgments

The authors would like to acknowledge the support provided by Fundação para a Ciência e a Tecnologia of Portugal (FCT) and IDMEC for its financial support via the projects LAETA Base Funding (DOI: 10.54499/UIDB/50022/2020) and 2023.12345.PEX (DOI: 10.54499/2023.12345.PEX).

Data availability

Data will be made available on request.

References

American Welding Society, 2019. AWS C1.1M/C1.1:2019 AMD1 – Recommended Practices For Resistance Welding.

Braun, M., Schubnell, J., Sarmast, A., et al., 2023. Mechanical behavior of additively and conventionally manufactured 316L stainless steel plates joined by gas metal arc welding. J. Mater. Res. Technol. 24, 1692–1705.

Calado, F.N., Pragana, J.P.M., Bragança, I.M.F., Silva, C.M.A., 2022. Resistance element welding of sandwich laminates with hidden inserts. Int. J. Adv. Manuf. Technol. 118 (5), 1565–1575.

Gornyakov, V., Sun, Y., Ding, J., Williams, S., 2022. Modelling and optimising hybrid process of wire arc additive manufacturing and high-pressure rolling. Mater. Des. 223, 111121.

Huysmans, S., Peeters, E., De Bruycker, E., De Prins, K., 2021. Weldability study of additive manufactured 316L austenitic stainless steel components – welding of AM with conventional 316L components. Weld. World 65 (7), 1415–1427.

International Organization for Standardization, 2016a. ISO 5182:2016 – resistance welding – materials for electrodes and ancillary equipment. ISO, Geneva, Switzerland.

International Organization for Standardization, 2016b. ISO 14270:2016 – Resistance Welding – Destructive Testing of Welds – Specimen Dimensions and Procedure For Cross Tension Testing of Resistance Spot Welds. ISO, Geneva, Switzerland.

International Organization for Standardization, 2016c. ISO 14273:2016 – Resistance Welding – Destructive Testing of Welds – Specimen Dimensions and Procedure For Tensile Shear Testing of Resistance Spot and Embossed Projection Welds. ISO, Geneva, Switzerland.

Jagadeesha, T., 2017. Experimental studies in weld nugget strength of resistance spot-welded 316L austenitic stainless steel sheet. Int. J. Adv. Manuf. Technol. 93 (1), 505–513.

Kim, S., Park, S., Kim, M., Kim, D.Y., Park, J., Yu, J., 2023. Weldability of additive manufactured stainless steel in resistance spot welding. Metals 13 (5), 837.

Lauwers, B., Klocke, F., Klink, A., Tekkaya, A.E., Neugebauer, R., Mcintosh, D., 2014. Hybrid processes in manufacturing. CIRP Ann. 63 (2), 561–583.
Li, B., Nagaraja, K.M., Zhang, R., Malik, A., Lu, H., Li, W., 2023. Integrating robotic wire arc additive manufacturing and machining: hybrid WAAM machining. Int. J. Adv. Manuf. Technol. 129 (7), 3247–3259.
Lippold, J.C., Kotecki, D.J., 2005. Welding Metallurgy and Weldability of Stainless Steels. Wiley-Interscience, Hoboken, NJ, USA.
Matilainen, V.P., Pekkarinen, J., Salminen, A., 2016. Weldability of additive manufactured stainless steel. Phys. Procedia 83, 808–817.
Mazar Atabaki, M., Ma, J., Yang, G., Xu, C., Chenier, P., Harooni, M., Kovacevic, R., 2016. Welding of stainless steels and other similar materials: methods and microstructural evolution. Mater. Sci. Eng. A 674, 573–597.
Merklein, M., Junker, D., Schaub, A., Neubauer, F., 2016. Hybrid additive manufacturing technologies – an analysis regarding potentials and applications. Phys. Procedia 83, 549–559.
Mokhtari, M., Pommier, P., Balcaen, Y., Alexis, J., 2021. Laser welding of AISI 316L stainless steel produced by additive manufacturing or by conventional processes. J. Manuf. Mater. Process. 5 (4), 136.
Pouranvari, M., 2011. Effect of welding current on the mechanical response of resistance spot welds of unequal thickness steel sheets in tensile-shear loading condition. Int. J. Multidiscip. Sci. Eng. 2 (6), 178–189.
Pragana, J.P.M., Bragança, I.M.F., Silva, C.M.A., Sampaio, R.F.V., Martins, P.A.F., 2023. Hybrid wire-arc additive manufacturing of conformal cooling channels: a feasibility study. Int. J. Precis. Eng. Manuf. – Green Technol. 10 (1), 45–57.
Pragana, J.P.M., Sampaio, R.F.V., Bragança, I.M.F., Silva, C.M.A., Martins, P.A.F., 2021. Hybrid metal additive manufacturing: a state-of-the-art review. Adv. Ind. Manuf. Eng. 2, 100032.
Rosado, P.M., Sampaio, R.F.V., Pragana, J.P.M., Bragança, I.M.F., Silva, C.M.A., Martins, P.A.F., 2024. Exploring wire-arc additive manufactured rivets for joining hybrid electrical busbars. J. Adv. Join. Process. 10, 100272.
Sampaio, R.F.V., Pragana, J.P.M., Bragança, I.M.F., Silva, C.M.A., Martins, P.A.F., 2023. Thermo-electrical performance of hybrid busbars: an experimental and numerical investigation. J. Mater. 237, 70–80.
Selmi, H., Brousseau, J., Caron-Guillemette, G., Goulet, S., Desjardins, J., Belzile, C., 2023. Weldability of 316L parts produced by metal additive manufacturing. J. Manuf. Mater. Process. 7 (2), 71.
Sitharaj, A., Arulmurugan, B., Veeraraghavan, V., Idhayaraja, S., Vivekanandh, S.R., Kavin, M., Kumaar, A.A., 2024. Hybridization in wire arc directed energy deposition of titanium alloys: a review. In: International Conference on Additive Manufacturing. Springer Nature Singapore, Singapore, pp. 441–465.
SWANTEC Software and Engineering ApS, 2019. SORPAS® 2D Version 13.5 user manual. June 2019.
Ucsnik, S.A., Kirov, G., 2011. New possibility for the connection of metal sheets and fiber reinforced plastics. Mater. Sci. Forum 690, 465–468.
Zhang, W., 2003. Design and implementation of software for resistance welding process simulations. SAE Trans. 556–564.
Zhu, Z., Dhokia, V.G., Nassehi, A., Newman, S.T., 2013. A review of hybrid manufacturing processes – state of the art and future perspectives. Int. J. Comput. Integr. Manuf. 26 (7), 596–615.